Marine Environmental Research 221 (2026) 108321

Contents lists available at ScienceDirect

Marine Environmental Research

journal homepage: www.elsevier.com/locate/marenvrev

Cyclonic surface circulation in the northern coast of the Gulf of Cádiz: insights from Lagrangian drifters and high-resolution models

Esther Luján-Amoraga [a,*], Carlos Román-Cascón [a], Juan Alberto Jiménez Rincón [b], Alfredo Izquierdo [a], Miguel Bruno [a], Águeda Vázquez [a], Paulo Relvas [c], Erwan Garel [d], Marina Bolado-Penagos [a]

[a] Department of Applied Physics, Faculty of Marine and Environmental Sciences, Marine Research Institute (INMAR), International Campus of Excellence of the Sea (CEI·MAR), University of Cadiz, Puerto Real, Cadiz, 11510, Spain
[b] Physical Oceanography Dept, Spanish Institute of Oceanography, Cádiz Oceanographic Center, Muelle de Levante s/n, Puerto Pesquero, Cádiz, 11006, Spain
[c] Centre of Marine Sciences (CCMAR), University of Algarve, Faro, 8005-139, Portugal
[d] Centre for Marine and Environmental Research (CIMA), University of Algarve, Faro, 8005-139, Portugal

ABSTRACT

This study presents direct *in situ* observational evidence of a cyclonic circulation cell east of Cape *Santa María* (CSM), in the northern Gulf of *Cádiz* (GoC). Three Lagrangian drifters deployed in October 2022 revealed a coherent cyclonic circulation cell with a characteristic diameter of approximately 40-45 km, consistently estimated from drifter trajectories and relative vorticity. Their trajectories showed alternating eastward and westward flows, modulated by wind variability, bathymetry, and mesoscale dynamics. Satellite observations showed a cooler, chlorophyll-*a* enriched core, consistent with upwelling and retention of enriched surface water masses within the circulation cell.

High-resolution WRF atmospheric simulations indicated alternating easterly and westerly wind regimes that were associated with reversals in coastal circulation. Westerly winds between 18th and 24th October produced positive Ekman pumping east of CSM, creating conditions favourable to the intensification of cyclonic circulation. The IBI ocean model reproduced the main structure of the circulation cell structure, including flow accelerations near the shelf edge, and indicated upward vertical motions within the cyclonic circulation cell.

A Lagrangian particle experiment suggested that the cyclonic cell favours both retention and offshore export of surface waters, with residence times of up to approximately 16 days. Overall, this study highlights the role of interactions between atmospheric forcing, bathymetry, and mesoscale dynamics in controlling small-scale surface circulation in the GoC, and underscores the value of integrating drifter observations, satellite data, and numerical models to characterize coastal dynamics.

1. Introduction

Ocean currents, including surface currents, influence many activities with significant socio-economic and environmental effects. These include fisheries, offshore energy production, and navigation (e.g., Aguiar et al., 2020). In terms of environmental impact, they affect the dispersion and transport of pollutants such as microplastics (e.g., Laiz et al., 2024) or oil spills, as well as the distribution of physicochemical variables and marine organisms (García et al., 2002). Beyond these practical implications, surface circulation plays a fundamental role in the redistribution of heat, mass, and energy, directly shaping climate, marine ecosystems, and productivity (Talley et al., 2011; Brink, 2016).

Large-scale circulation processes and patterns in the open ocean are currently well characterized (Fu et al., 2010). However, processes occurring at smaller spatial and temporal scales, particularly in coastal areas, are more challenging to characterize due to the complexity of the interactions between local, regional, and remote factors (García et al., 2002; Mulero-Martínez et al., 2021).

In this context, mesoscale and submesoscale processes, with horizontal scales of approximately 1-100 km play an important role in regulating surface circulation and redistributing mass, heat, tracers, and nutrients, with direct consequences for marine productivity and cross-shelf exchanges (Gomis et al., 2001; McWilliams, 2016; Cravo et al., 2013; Dong et al., 2025). Surface wind speed and direction are the main drivers of surface ocean circulation at these scales, making them essential variables in the Global Climate Observing System (GCOS, 2016). Upwelling systems represent paradigmatic settings where mesoscale dynamics, including coastal jets, eddies, filaments, and

This article is part of a special issue entitled: Marine Processes and Humans MERE published in Marine Environmental Research.

* Corresponding author.
E-mail address: esther.lujan@uca.es (E. Luján-Amoraga).

https://doi.org/10.1016/j.marenvres.2026.108321
Received 13 November 2025; Received in revised form 29 June 2026; Accepted 29 July 2026
Available online 30 July 2026

recirculation cells, strongly modulate cross-shelf transport and biological productivity (Relvas et al., 2007; Teles-Machado et al., 2016).

This work focuses on the Gulf of *Cádiz* (hereinafter, GoC), a region where oceanographic research has traditionally focused on wind and pressure as the two main factors affecting surface currents (Garel et al., 2016; Oliveira et al., 2021; Sirviente et al., 2023). This region borders the coasts of the southwest of the Iberian Peninsula and extends from Cape *São Vicente* (CSV) to the westernmost part of the Strait of Gibraltar (SoG). It is a complex oceanic area influenced by a range of local and remote forcings (García et al., 2002; Mulero-Martínez et al., 2021). Most studies have focused on deep circulation and on the influence of Mediterranean Water outflow into the Atlantic (e.g., Sánchez-Leal et al., 2020; Rautenbach et al., 2024). In contrast, studies on surface or coastal circulation are less abundant, although they have increased in recent years (e.g., Peliz et al., 2009; de Oliveira-Júnior et al., 2022; Sirviente et al., 2023; de Oliveira Júnior et al., 2024). Moreover, much of the research on coastal surface circulation in the GoC has been based on satellite-derived sea surface temperature (SST) data (Fiúza, 1983; Sánchez and Relvas, 2003; Vargas et al., 2003). As a result, the small-scale surface dynamics of the GoC continental shelf remain poorly constrained by direct observations.

On the GoC continental shelf, coastal dynamics are strongly influenced by bathymetry and wind. The shelf can be divided into two regions separated by Cape *Santa María* (CSM): to the west, the shelf is narrower, less than 25 km wide, whereas to the east it widens to about 40 km, creating a gentler slope and a different circulation pattern (García-Lafuente et al., 2006). This topographic contrast plays a key role in shaping local circulation patterns and modulating the development of mesoscale structures.

The wind regime in the GoC is complex and variable, dominated by westerly winds, locally known as *Poniente*, and easterly winds, locally known as *Levante*. These winds play a key role in coastal circulation, the development of oceanic structures, and upwelling processes. Northerly winds are also common along the Iberian margin and contribute significantly to coastal upwelling processes (e.g., Soares et al., 2014). At CSV, northerly winds induce coastal upwelling events that occur frequently throughout the year (Ruiz and Navarro, 2006; Cravo et al., 2013). In the CSM area, upwelling responds rapidly to changes in the wind regime, generating alongshore pressure gradients and sea-level slopes (Criado-Aldeanueva et al., 2006; Relvas and Barton, 2002; de Oliveira Júnior et al., 2022).

During easterly wind episodes, mesoscale and submesoscale structures such as the Coastal Countercurrents (CCC) form in the GoC, flowing westwards close to the coast and often associated with upwelling zones (García-Lafuente et al., 2006; de Oliveira Júnior et al., 2021; Sirviente et al., 2023). The CCC arises from coastal pressure-gradient imbalances driven by the wind field (Garel et al., 2016; Criado-Aldeanueva et al., 2006). According to Garel et al. (2016), this current appears approximately 40% of the time. In some cases, the pressure gradients that favour CCC formation originate from the relaxation of westerly winds rather than from easterly forcing (Garel et al., 2016), although other studies suggest that, without easterly winds, the CCC does not become clearly established (Teles-Machado et al., 2007). During summer, the CCC is associated with the westward propagation of warm waters over the continental shelf and along its outer edge on the southern coasts of Portugal and Spain (Relvas and Barton, 2002, 2005; Sánchez et al., 2006).

Another mesoscale feature induced by easterlies winds in the GoC is the formation of shallow, surface-intensified anticyclonic eddies. These arise when strong easterlies winds, channelled through the SoG, interact with the upper-ocean thermohaline structure, giving rise to the so-called Levanter Anticyclones (Peliz et al., 2014). Although transient, these energetic structures can significantly influence surface circulation beyond the continental shelf.

Regarding cyclonic circulation, García-Lafuente et al. (2006) described the inner shelf circulation in the GoC as consisting of two cyclonic gyres that can connect under favourable wind conditions: one located in the eastern sector, resulting from geostrophic adjustment due to the density gradient between the cold jet and the warmer inner-shelf waters; and another located in the western part, related to the wind-stress response in the CSV area (Relvas and Barton, 2005).

Despite considerable progress, studies analysing coastal circulation in the GoC with high temporal and spatial resolution data remain scarce. Among these are investigations using Acoustic Doppler Current Profiler (ADCP) (García-Lafuente et al., 2006; Criado-Aldeanueva et al., 2006) and high-frequency radar (HFR) measurements (de Oliveira Júnior et al., 2022; Sirviente et al., 2023). However, further observations are still required to accurately characterize small-scale surface processes.

In this work, we combine *in situ* measurements from Lagrangian drifters, satellite data, and high-resolution atmospheric and oceanographic models outputs from the Weather Research and Forecasting (WRF) mesoscale model and Iberian–Biscay–Irish (IBI) ocean model. This integrated approach enables the analysis of the dynamic response of surface circulation to atmospheric forcing in the GoC. Specifically, the study focuses on a case in which a well-defined cyclonic circulation cell developed east of CSM. This event was captured by Lagrangian drifter measurements and further analysed using satellite observations and numerical model outputs.

The paper is structured as follows. Section 2 describes the material and methods. Section 3 presents the main results obtained from different sources, while Section 4 discusses the findings. Finally, Section 5 summarises the main conclusions.

2. Material and methods

This work combines *in situ* observations, satellite products, and high-resolution numerical model outputs to analyse surface circulation variability over the GoC continental shelf and its relationship with the atmospheric forcing. This section describes the datasets and methods used, including Lagrangian drifter observations and particle simulations, satellite-derived products, and atmospheric and oceanographic model outputs.

2.1. In situ measurements: Lagrangian drifters

Three Lagrangian drifters were deployed east of CSM on 12th October 2022 to study surface currents in the northern GoC (Fig. 1). One drifter, LCA00565 (green circle in Fig. 1), was released at 37.080° N, 7.476° W, over the 25 m isobath, whereas the other two drifters, LCA00564 and LCA00566 (red and blue circles in Fig. 1, respectively), were released at 36.993° N, 7.423° W, over the 100 m isobath. All drifters were equipped with approximately 50 cm drogue sails and a 1 m tether to reduce the direct impact of wind on their movement.

The drifters were Coastal Nomad units manufactured by SouthTEK (www.southtek.com), equipped with GSM coverage and GPS position transmission at pre-configured intervals. Previous studies have used the same drifter model in coastal applications (e.g., Bolado-Penagos et al., 2020; Sala et al., 2018; Ribotti et al., 2023). In this study, the drifters were programmed to record their position hourly. The resulting trajectories were analysed to characterize surface circulation and to identify potential mesoscale and submesoscale structures in a region where *in situ* observations are scarce and HFR coverage is limited (Mulero-Martínez et al., 2021; Sirviente et al., 2023).

A quality control procedure was applied to remove erroneous records that could introduce uncertainty into the trajectory and velocity estimates. Time gaps caused by intermittent transmission failures occasionally produced unrealistically high implied speeds between non-consecutive fixes. Records implying speeds greater than $1.0\,\mathrm{m\,s^{-1}}$ were therefore removed. A common period of reliable operation across the three drifters (from 12 to 24 October 2022) was then selected to allow simultaneous comparison of their trajectories.

The distance travelled between consecutive hourly positions was

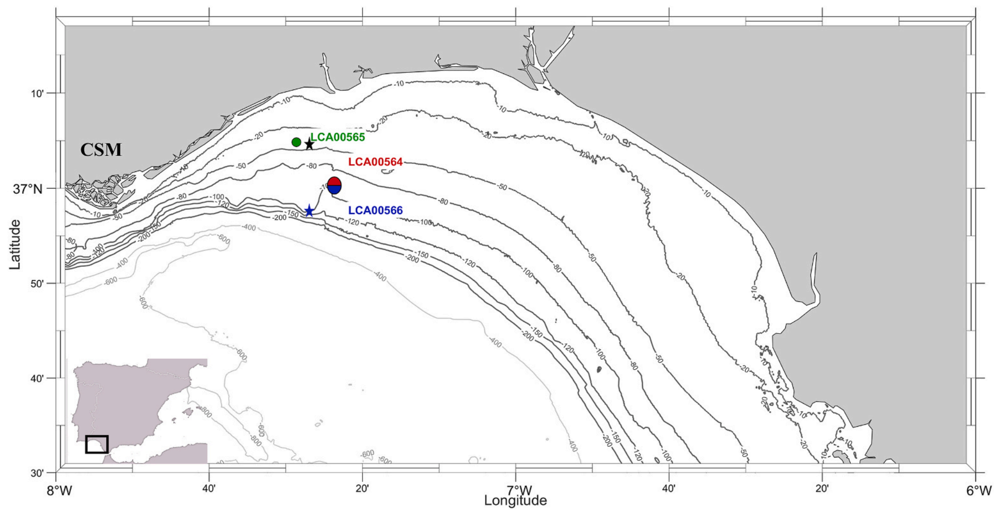

Fig. 1. Map of the study area showing the deployment positions of the three Lagrangian drifters. Drifter LCA00565 was released over the 25 m isobath (green), whereas drifters LCA00564 and LCA00566 were released over the 100 m isobath (red and blue, respectively). The blue star and black stars indicate the particle-release locations used in the Lagrangian simulations. (For interpretation of the references to colour in this figure legend, the reader is referred to the Web version of this article.)

calculated for each drifter, and the corresponding mean velocity was obtained by dividing this distance by the time interval of 1 h. The main variables used in the analysis were therefore drifter position, trajectory and velocity. The drifter codes, deployment positions and depths, final records, and operational durations are summarised in Table 1.

2.2. Meteorological characterization

To analyse meteorological conditions during the study period, wind fields from the Weather Research and Forecasting (WRF) mesoscale atmospheric model were used to assess their potential influence on surface currents.

WRF is a numerical mesoscale atmospheric model widely used for both research and operational applications. It was developed by several institutions, including the National Center for Atmospheric Research (NCAR, 2023). Its flexibility allows the simulation of atmospheric processes across scales ranging from tens of metres to thousands of kilometres, under either real or idealised conditions, making it a robust tool for atmospheric research and operational forecasting.

In this study, WRF version 4.2 was used (Skamarock et al., 2019), configured specifically for the GoC area. The main technical configuration parameters are summarised in Table 2.

Hourly WRF outputs of wind speed and direction were analysed for the period from 5th to 25th October 2022. These data were used to identify changes in the wind regime and to provide a fine-scale meteorological characterization of the atmospheric forcing during the drifters observations. Particular attention was given to intervals dominated by easterly winds, which are often well established in the SoG and the GoC, and to periods characterized by westerly winds in the northern GoC.

WRF outputs were also analysed to identify upwelling-favourable wind conditions and to estimate Ekman transport and Ekman pumping east of CSM. The MATLAB Climate Data Toolbox (CDT, Greene et al., 2019) was used to estimate Ekman transport from wind-stress fields. The horizontal momentum balance equations describing the Ekman layer are expressed as:

$$fu = \frac{1}{\rho}\frac{\partial \tau_y}{\partial z}, fv = -\frac{1}{\rho}\frac{\partial \tau_x}{\partial z} \quad \text{Eq. 1}$$

where f is the Coriolis parameter, ρ is seawater density, and τx and τy are the zonal and meridional wind stresses, respectively.

The wind-stress components were computed as:

$$\tau_x = \rho_a Cd|V_a|u_a, \tau_y = \rho_a Cd|V_a|v_a \quad \text{Eq. 2}$$

where Va = (u_a, v_a) is the wind velocity, ρ_a is the air density, and C_d the drag coefficient, calculated following Large and Pond (1981) and modified by Trenberth et al. (1990) for low wind speeds:

$$C_d = 0.00218 \text{ for } |V_a| \leq 1 \text{ m s}^{-1}$$

$$C_d = (0.62 + 1.56\,|V_a| - 1)\ 0.001 \text{ for } 1 \text{ m s}^{-1} < |V_a| < 3 \text{ m s}^{-1}$$

$$C_d = 0.00114 \text{ for } 3 \text{ m s}^{-1} \leq |V_a| < 10 \text{ m s}^{-1}$$

Table 1
Summary of the three Lagrangian drifters in this study: drifter code, deployment position, deployment date and isobath, final record, and operational duration.

Drifter code	Deployment position	Deployment date and isobath	Final record	Operational duration
LCA00564	36.993° N 7.423° W	12/10/2022 100 m	15/12/2022	64
LCA00565	37.080° N 7.476° W	12/10/2022 25 m	29/10/2022	18
LCA00566	36.993° N 7.423° W	12/10/2022 100 m	23/10/2022	12

Table 2
Technical configuration parameters of the WRF model used in this study.

WRF (Version 4.2)	
Central point	36.490° N, 6.960° W
Number of domains	3
Horizontal resolution	9, 3, 1 km
Number of vertical levels	51
Start simulation	05/10/2022 00:00
End of simulation	25/10/2022 00:00
Time step	54 s
Microphysics scheme	WRF Single Moment 3, (Hong et al., 2004)
Boundary layer scheme	Yonsei University (YSU), (Hong et al., 2006)
Shortwave radiation scheme	Dudhia (Dudhia, 1989)
Longwave radiation scheme	Rapid Radiative Transfer Model, (Mlawer et al., 1997)
Ground-surface scheme	Noah Land Surface Model (Mitchell et al, 2005)
Boundary conditions	NCEP-FNL 0. 25° (UCAR\NCAR, 2015)

$C_d = (0.49 + 0.065|V_a|)\,0.001$ for $|V_a| \geq 10\ \mathrm{m\ s^{-1}}$

Integrating Eq. (1) with respect to depth yields the Ekman transport components:

$$Ek_{Tx} = \frac{\tau_y}{\rho f}, Ek_{Ty} = \frac{\tau_x}{\rho f} \qquad \text{Eq. 3}$$

In the northern Hemisphere, Ekman transport is directed 90° to the right of the wind. When winds blow parallel to the coast, offshore Ekman transport promotes divergence and upwelling, whereas onshore transport favours convergence and downwelling.

The vertical velocities associated with Ekman pumping (w_{Ek}) were calculated from the curl of the wind-stress field:

$$w_{Ek} = \hat{k} \cdot \left(\frac{1}{\rho f}\right) \nabla x \vec{\tau} = \left(\frac{1}{\rho f}\right)\left(\frac{\partial \tau_y}{\partial x} - \frac{\partial \tau_x}{\partial y}\right) \qquad \text{Eq. 4}$$

Positive values of w_{Ek} indicate upward motion associated with upwelling, whereas negative values indicate downward motion associated with downwelling or Ekman suction.

2.3. Oceanographic characterization

To provide a more complete oceanographic characterization of the study area during the drifter-deployment period, satellite products and numerical model outputs were analysed. These included sea surface temperature (SST), surface chlorophyll-a (Chl-a) concentration, sea-level anomaly (SLA), and ocean current fields.

2.3.1. Satellite products

SST data were obtained from the ODYSSEA L4 product, with hourly temporal resolution and 0.05° spatial resolution, available at https://doi.org/10.48670/mds-00345). Surface chlorophyll-a (Chl-a) concentration was derived from the Copernicus-GlobColour L4 product, with daily temporal resolution of approximately 4 km spatial resolution, available at https://doi.org/10.48670/moi-00281. Both datasets were analysed for the period from 12th to 24th October 2022. These products were used to identify spatial and temporal variations in SST and Chl-a associated with mesoscale and submesoscale structures, including coastal upwelling-related patterns, which are typically linked to colder waters and enhanced phytoplankton biomass (Reggiannini et al., 2021; Sydeman et al., 2014).

SLA data were obtained from the Copernicus DUACS delayed-time gridded altimeter product, with daily temporal resolution and 0.125° spatial resolution, available at https://doi.org/10.48670/moi-00148. This product merges observations from multiple satellite missions and provides consistent estimates of sea-surface height relative to the long-term mean. In this study, SLA fields were analysed over the GoC for the period from 12th to 24th October 2022 to evaluate the surface expression of the cyclonic circulation cell detected by the drifters. The SLA fields were also used together with IBI model outputs to assess the consistency between observed and simulated surface circulation patterns.

2.3.2. Numerical model

Surface and vertical current velocities were obtained from the Iberian–Biscay–Irish (IBI) Ocean Physics Analysis model (product ID: *IBI_ANALYSISFORECAST_PHY_005_001*), available at https://doi.org/10.48670/moi-00027. The high-resolution ocean analysis and forecasting product provided by the Copernicus Marine Environment Monitoring Service (CMEMS). Its hydrodynamic simulations include high-frequency processes such as tidal forcing, surges, atmospheric forcing, river discharge, and wave forcing in forecast mode, enabling a detailed representation of regional-scale ocean dynamics. The product integrates the last two years of historical best estimates with near-real-time forecasts updated daily, ensuring consistent and continuous information on ocean variability. The product has a horizontal resolution of approximately 3 km and provides hourly mean fields, 15-min instantaneous surface variables, and daily and monthly three-dimensional fields. In this study, surface current fields, represented by the *uo* and *vo* velocity components, were analysed to compare simulated circulation with the drifter observations and to assess the model's ability to reproduce the observed surface dynamics in the GoC. To quantify model performance, a virtual drifter was simulated for each observed drifter using the same release position and time, and advected using only the IBI surface velocity field. Model performance was then evaluated using two complementary Lagrangian metrics: the separation distance between observed and simulated trajectories at each time step, and the dimensionless skill score proposed by Liu and Weisberg (2011), defined as:

$$s(n) = 1 - \frac{\sum d(i)}{\sum l(i)} \qquad \text{Eq. 5}$$

where *d(i)* is the separation distance at time step *i* and *l(i)* is the cumulative path length travelled by the observed drifter up to that time step. This skill score ranges from 1, indicating perfect agreement, to negative values when the separation distance exceeds the cumulative length of the observed trajectory) (Liu and Weisberg, 2011).

In addition, the IBI model was used to calculate relative vorticity within the study area during the period analysed, in order to examine the possible role of bathymetric gradients in modulating the rotational dynamics of the cyclonic circulation cell (see Fig. S2).

2.3.3. Lagrangian analysis using OceanParcels

To investigate particle transport and retention patterns, a Lagrangian analysis was carried out using the *OceanParcels* framework (e.g., Delandmeter and van Sebille, 2019). This tool allows passive particle trajectories to be simulated by advecting particles with ocean currents fields. In this study, horizontal velocity fields from the CMEMS IBI model were used as forcing data. Particles were released at predefined locations and advected for 12th to 27th October 2022 allowing the identification of retention areas, dispersion pathways, and connectivity between regions.

Particles were released at two predefined locations, indicated by the blue and the black stars in Fig. 1). A total of 32 particles were released from each location, with one particle released every 12 h between 12th and 27th October 2022. Particles were advected at the surface to represent near-surface transport.

Particle trajectories were computed using the fourth order Runge-Kutta advection scheme (AdvectionRK4) implemented in OceanParcels (v3.1.0), with particle positions saved hourly. Bilinear spatial and linear temporal interpolation were applied to the velocity fields. When particles reached the coastline, they were not removed from the simulation. Instead, a coastline-repulsion kernel prevented them from crossing onto land by displacing them back into the ocean, after which they continued to follow the local velocity field. Three regions were then defined for the subsequent analysis: OFF-SHELF, WESTERN SHELF and CYCLONIC CELL.

3. Results

3.1. Drifters' trajectory: surface oceanic circulation

The Lagrangian drifters deployed in the northern GoC (Fig. 2) revealed a cyclonic (anticlockwise) surface circulation, indicating the presence of a well-defined cyclonic circulation cell. The horizontal scale of the structure was estimated independently from two sources, (i) the drifter trajectories and (ii) the mean relative vorticity field from the IBI model (Fig. S1). Both estimates yielded a consistent diameter of approximately 40-45 km.

Drifter LCA00565, released over the continental shelf (green circle in Fig.1, ~25 m isobath), initially moved southwestward and then turned

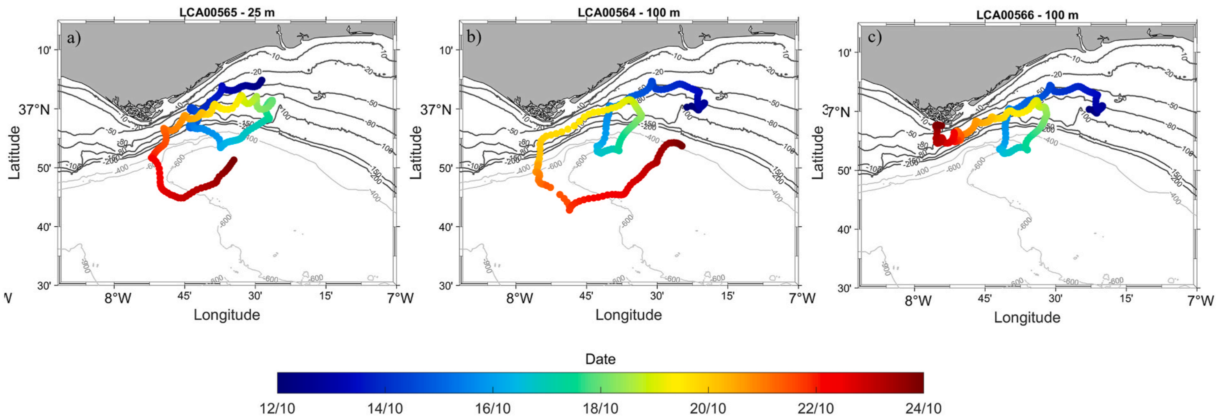

Fig. 2. Drifter trajectories during the common observation period. Colours indicate the progression of time from 12 October 2022 (blue) to 23 October 2022 (red). Bathymetric data are from EMODnet DTM 2018; Bryant, 2016). (For interpretation of the references to colour in this figure legend, the reader is referred to the Web version of this article.)

eastward, describing a cyclonic loop in approximately 7 days (Fig. 2a). It subsequently drifted westward and southward before turning northeast again, completing almost two cyclonic rotations.

The drifters deployed in deeper waters, LCA00564 and LCA00566 (red and blue circles in Fig.1, ~100 m isobath), showed a similar pattern, although with higher speeds, up to 0.6 m s^{-1}, and slight variations in their trajectories. LCA00564 reached the CSM region earlier, on 18th October (yellow in Fig. 2b), whereas LCA00566 was more strongly influenced by coastal currents that modified its path (Fig. 2c). As a result, LCA00566 completed only one cyclonic rotation before moving towards the coast in the vicinity of the CSM.

Overall, the drifters described a cyclonic, anticlockwise rotation, alternately leaving and re-entering the shelf area. Over the shelf, they moved eastward following the coastal current. After leaving the shelf, they turned southeastward, completing the outer branch of the cyclonic circulation cell. Upon re-entering the shelf, around the 80 m isobath, their trajectories turned westward again, closing the cyclonic loop, except in the case of LCA00566.

The analysis of the drifter's velocity reveals that the most significant changes occurred during transitions between the continental shelf and the slope (Fig. 3). Drifter LCA00564 accelerated while crossing the narrow section of the shelf off CSM (Fig. 3b), completing a shorter and faster loop was likely influenced by an inner branch of the cyclonic circulation cell. Because it travelled a shorter distance, this drifter completed the rotation over a shorter time interval, with a clear acceleration near CSM on 19th October, when it reached 0.6 m s^{-1}.

Drifters LCA00565 and LCA00566 showed a similar evolution, with noticeable accelerations shortly after leaving the shelf (Fig. 3a–c), likely associated with advection by an eastward branch of the surface current. Both drifters accelerated again when redirected westward during re-entry onto the shelf, suggesting the influence of the outer branch of the cyclonic circulation cell. Drifter LCA00565 exhibited two main velocity peaks above 0.4 m s^{-1}, on 16th and 19th October, and LCA00566 followed a comparable pattern, consistent with the dynamics observed within the cyclonic circulation cell.

3.2. *Meteorological characterization of the period*

As previously mentioned, the wind regime is one of the main drivers of surface circulation in the GoC and is highly variable in both space and time. To characterize the atmospheric conditions during the observation period, WRF model outputs were from 5th to 24th October 2022.

The results revealed alternating episodes of westerly–southwesterly and easterly-northeasterly winds throughout the study period. To this spatial variability, two regions with contrasting atmospheric conditions were selected: the northern GoC, where the drifters were deployed, and the SoG. These regions frequently show different, and sometimes opposite, wind directions on the same day. This contrast likely reflects

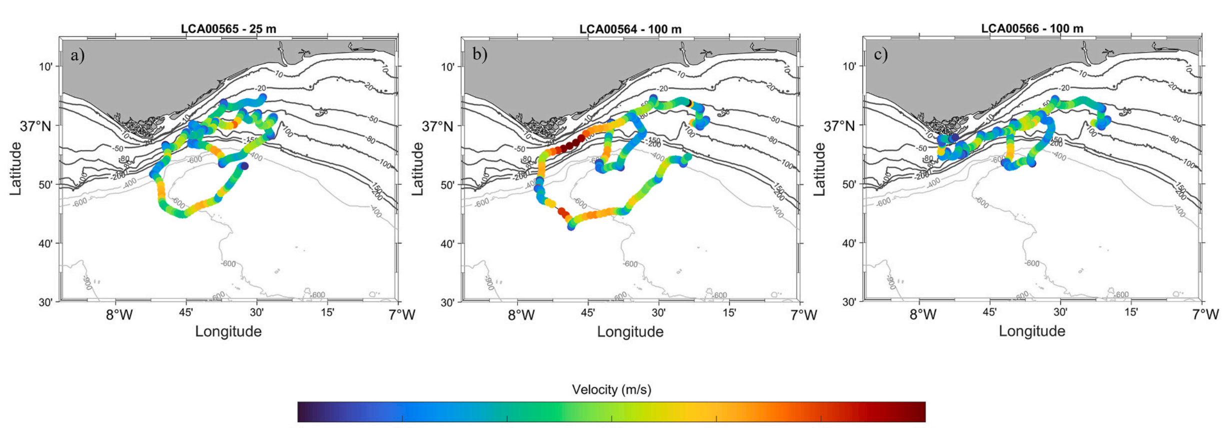

Fig. 3. Drifters trajectories followed overlaid on the bathymetry of the study area. Colours indicate drifter velocity along each trajectory. (For interpretation of the references to colour in this figure legend, the reader is referred to the Web version of this article.)

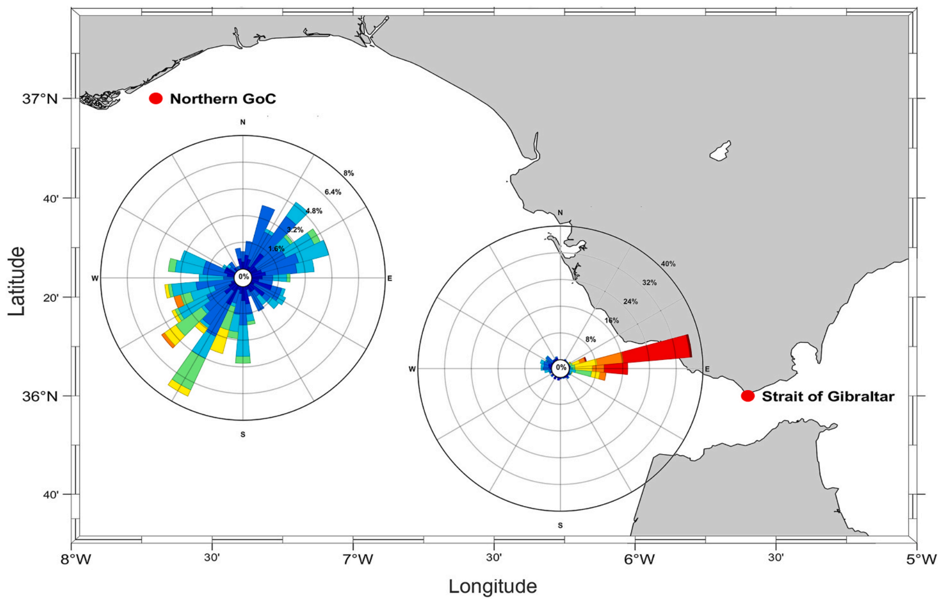

Fig. 4. Map of the Gulf of Cádiz (GoC) showing the two regions where wind roses were computed from WRF model data for the period 5–24 October 2022: one representative point in the northern GoC (37.0° N, 7.7° W) and another in the Strait of Gibraltar (36.0° N, 5.6° W).

Table 3
Predominant wind directions during October 2022 in the Strait of Gibraltar (SoG) and in the northern Gulf of Cádiz (GoC, east of Cape Santa María). The table shows the most frequent wind direction in each region for each date or date range.

Date	SoG	North of GoC
5 – 8 October 2022	E	NE
9 October 2022	E	NE
10 October 2022	W	SW/W
11 October 2022	E	NE
12 - 13 October 2022	E	N/NE
14 October 2022	E	NE
15 October 2022	E	SW/W
16 – 17 October 2022	E	NE
18 – 19 October 2022	E	S/SW
20 – 21 October 2022	W	SW/W
22 October 2022	E	S/SW
23 October 2022	W	SW/W
24 October 2022	E	S/SW

the influence of local and regional atmospheric dynamics, including thermally driven circulations in the northern GoC under weaker synoptic forcing than in the SoG.This spatial contrast is clearly illustrated in Fig. 4, where the wind roses show the predominant wind regimes in each region during the study period. The northern GoC was characterized by alternating southwesterly and northeasterly winds, whereas the SoG showed a more persistent prevalence of easterlies conditions.

A more detailed summary of this variability is provided in Table 3, which lists the predominant wind directions during October 2022 in the SoG and in the northern GoC, east of CSM (Fig. 4). The table highlights the alternating and localised nature of the atmospheric forcing affecting the observed surface circulation.

3.3. Oceanographic characterization

3.3.1. Chlorophyll-a concentration and SST

During the period covered by the drifter observations, surface Chl-*a* concentration was analysed together with the drifter trajectories. The results show that surface Chl-*a* concentrations were higher within the region where the drifters described the cyclonic circulation cell than in the surrounding waters, except for the nearshore zone. Maximum values coinciding were located within the area enclosed by the trajectories (Fig. 5). This distribution suggests that the circulation cell may favour the retention and accumulation of biologically enriched surface waters.

A filament of enhanced Chl-*a* concentration was also identified, following a spatial pattern similar to that of the drifter paths, particularly between 14th and 22nd October (Fig. 5a–e). This feature appears to be associated with one branch of the cyclonic circulation cell and suggests transport of Chl-*a*-rich surface waters from the coastal zone towards more oceanic regions beyond the continental shelf. The elevated Chl-*a* concentrations are not necessarily indicative of local production alone, but may also reflect the advection of nutrient-rich coastal or upwelled waters towards the open sea.

Fig. 6 shows the evolution of SST together with the drifters trajectories. Throughout the study period, a core of cooler waters (bluish and greenish tones) was associated with the cyclonic circulation cell outlined by the drifter trajectories.

During the first part of the study period (14th–18th October), the cold-water core appears separated from the coast, delimiting a cyclonic structure confined offshore (Fig. 6a–c), consistent with the position of the drifters along the outer branch of the cyclonic circulation cell. This pattern suggests the possible presence of an upward transport associated with the cyclonic circulation cell, favouring the appearance of cooler and potentially nutrient-rich water near the surface. In the following days (20th–24th October), the cool-water region progressively shifted to the coast (Fig. 6d–f), coinciding with a strengthening of the wind component favourable to coastal upwelling. At the same time, a band of warmer waters (orange tones) is observed along the eastern coast of the GoC, with temperature differences of up to 2 °C relative to the western sector. This warm area gradually propagated westward during the analysed period.

3.3.2. Upwelling event

Based on these oceanographic observations described above, the evolution of the wind conditions preceding the coastal accumulation of cold waters was analysed to assess their possible role in the development of upwelling conditions and in the evolution of the cyclonic circulation cell. As previously mentioned, westerly to southwesterly winds favour upwelling along the eastern flank of the CSM. According to the wind

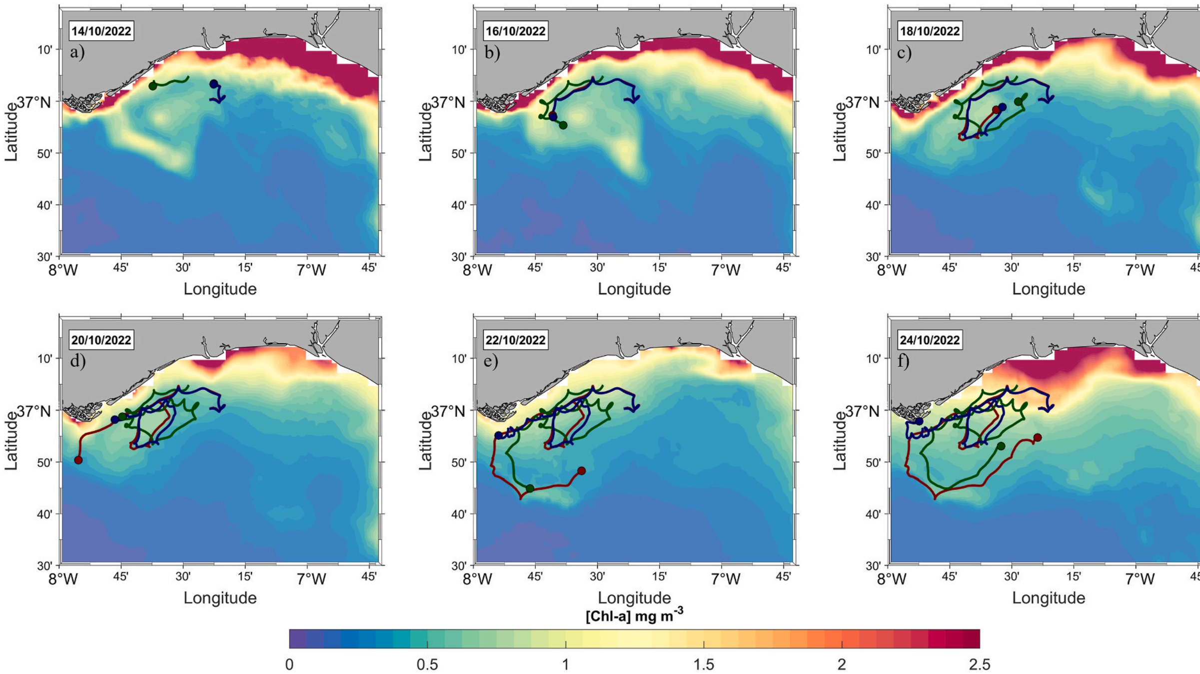

Fig. 5. Surface chlorophyll-a concentration (Chl-a, mg m^{-3}) from 14th to 24th October. Coloured lines represent the trajectories of the three drifters from their release on 12th October to the date shown in each panel: green (LCA00565), red (LCA00564), and blue (LCA00566). (For interpretation of the references to colour in this figure legend, the reader is referred to the Web version of this article.)

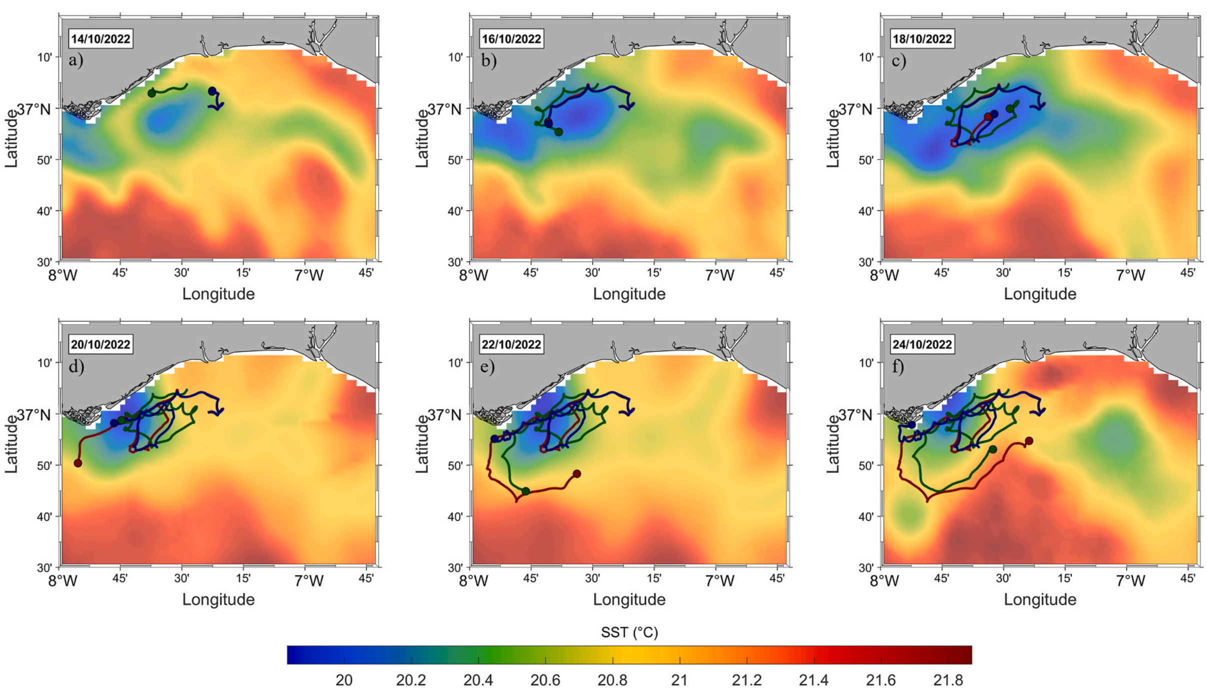

Fig. 6. Sea surface temperature (SST, °C) from 14th to 24th October 2022. Coloured lines represent the trajectories of the three drifters from their release on 12th October to the date shown in each panel: green (LCA00565), red (LCA00564), and blue (LCA00566). (For interpretation of the references to colour in this figure legend, the reader is referred to the Web version of this article.)

patterns summarised in Table 3, such winds predominated between 18th and 24th October 2022; therefore, Ekman transport and Ekman pumping were estimated for this period.

The results, shown in Fig. 7, display a spatial pattern consistent with the development of a coastal upwelling event in the GoC. From 18th October onwards, positive Ekman pumping values (reddish colours) intensified off the eastern coast of the GoC, reaching vertical velocities of up to $4{\cdot}10^{-5}$ m s^{-1}, consistent with the upward movement of subsurface water masses. At the same time, the Ekman transport fields reveal a net flow directed towards the southeast, resulting from the 90° deflection to the right of the wind direction, which is characteristic of an upwelling-favourable regime in the region.

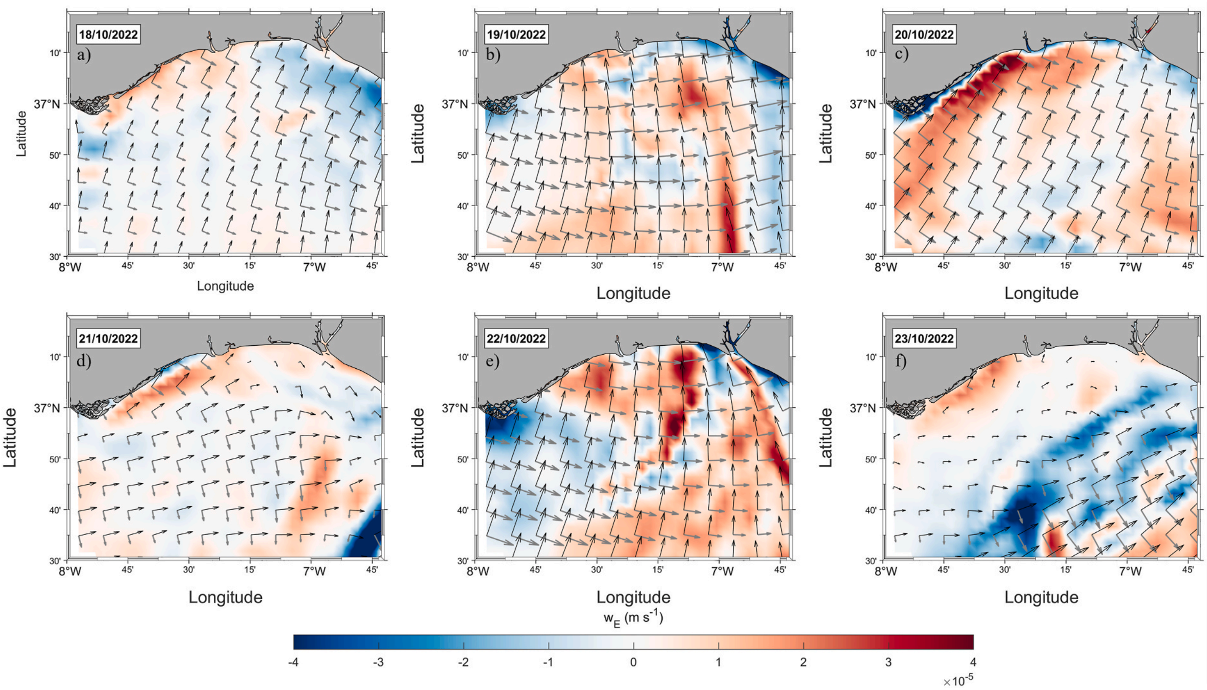

Fig. 7. Ekman transport and Ekman pumping vertical velocity (w_E, m s^{-1}) from 18thto 23rd October 2022. Black arrows indicate wind direction, and grey arrows indicate the direction of Ekman transport. Coloured contours show the vertical velocity associated with Ekman pumping, with positive values in red. (For interpretation of the references to colour in this figure legend, the reader is referred to the Web version of this article.)

This wind-driven surface transport would favour the ascent of cooler and potentially nutrient-rich waters near the coast and may also have contributed to the recirculation of the drifters, reinforcing the cyclonic movement observed in Fig. 2. In particular, the interaction between coastal upwelling and the cyclonic circulation cell may have favoured the confinement of cold waters near the coast. These results suggest that the atmospheric forcing played an important role in the evolution of the cyclonic circulation cell observed east of the CSM, modulating the redistribution of surface water masses and the trajectories of the drifters.

3.4. Comparison with the IBI model

High-resolution numerical models provide a valuable complement to *in situ* observations, as they allow the spatial and temporal variability of

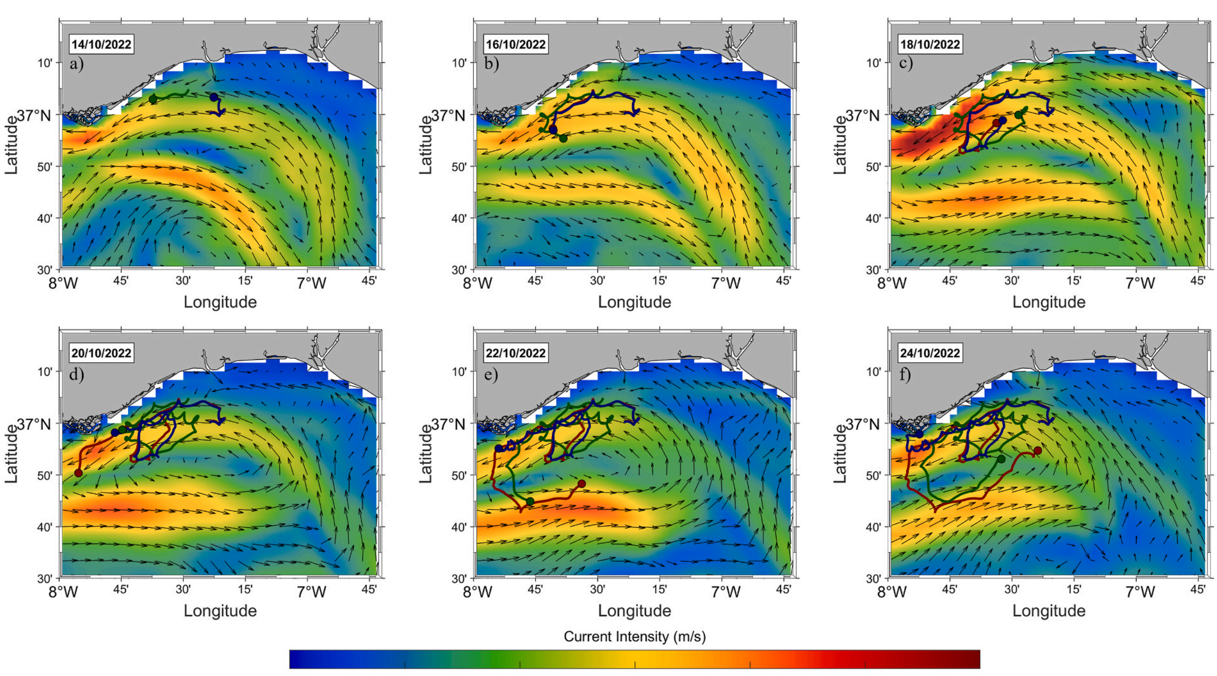

Fig. 8. Surface current speed (m s^{-1}) and direction simulated by the IBI model from 14th to 24th October2022. Coloured lines represent the trajectories of the three drifters from their release on 12th October 2022 to the date shown in each panel: green (LCA00565), red (LCA00564), and blue (LCA00566). (For interpretation of the references to colour in this figure legend, the reader is referred to the Web version of this article.)

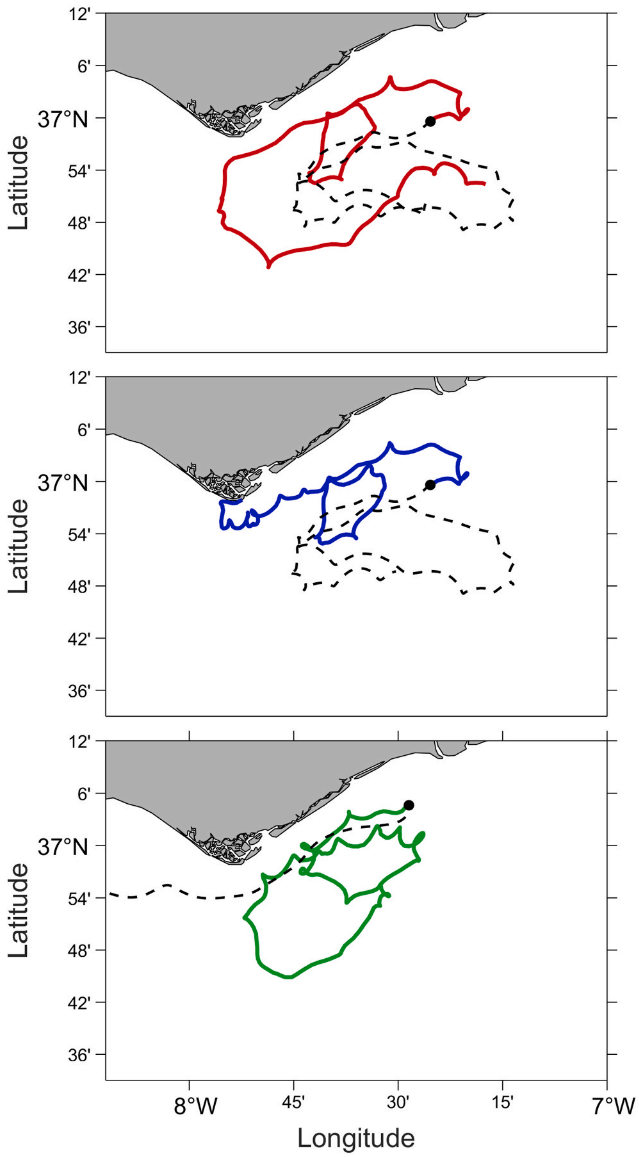

Fig. 9. Observed and IBI-simulated trajectories for each drifter from 12th to 24th October 2022. Coloured lines represent the observed drifter trajectories: green for LCA00565, red for LCA00564, and blue for LCA00566. Black dashed lines represent the corresponding IBI-simulated trajectories. Black dots indicate the release positions. (For interpretation of the references to colour in this figure legend, the reader is referred to the Web version of this article.)

oceanographic processes to be examined beyond the period and locations directly sampled by the drifters. In this section, the IBI model was used to assess the consistency between the observed drifter trajectories and the simulated surface circulation during the study period. characterization.

To evaluate whether the IBI model reproduce the main surface circulation patterns observed by the drifters, surface current fields corresponding to the same observation period were analysed. Fig. 8 shows both the direction and intensity of the surface currents simulated by the IBI model, superimposed on the Lagrangian drifters trajectories. The model reproduces the main features of the observed surface circulation in the study area, including the cyclonic circulation cell identified east of the CSM. However, the simulated structure, particularly during the first cyclonic rotation described by the drifters, appears slightly displaced southwards relative to the observed trajectories. This displacement is likely related to the limited ability of the model, with a horizontal resolution of approximately 3 km, to fully resolve coastal processes and fine-scale bathymetric effects. This limitation should therefore be considered when interpreting of the detailed structure of the simulated circulation.

Despite this displacement, the simulated current speed ares generally consistent with the values derived from the drifter observations (see Fig. 3). The model shows higher current speeds along the periphery of the cyclonic circulation cell and weaker flows at its centre, which is consistent with a recirculating structure. Furthermore, the model also reproduces zones of flow acceleration close to CSM and near the shelf re-entry region, coinciding with the main bathymetric transitions identified from the drifter trajectories.

The qualitative agreement between the observed and simulated circulation was further assessed using a Lagrangian comparison. For each observed drifter, a virtual drifter was released from the same position and at the same time and advected using only the IBI surface velocity field (Fig. 9). The model reproduced the recirculating nature of the flow for the two drifters released over the 100 m isobath, LCA00564 and LCA00566. In contrast, the model did not reproduce the observed cyclonic trajectory of LCA00565, which was released over the shallower continental shelf.

The model performance varied substantially among drifters and through time. The separation-distance analysis (Fig. 10) shows that, for LCA00564 and LCA00566, the simulated trajectories reproduced the general circulation pattern but were displaced southwards, with separation distances generally below 40 km during much of the comparison period. In contrast, LCA00565 showed poor agreement with the simulated trajectory, with the separation distance increasing progressively and reaching approximately 130 km by the end of the analysis period. This indicates that the model performed better for drifters deployed near the shelf edge than for the drifter released in shallow nearshore waters.

This contrast was also reflected in the Liu and Weisberg (2011) skill scores. The model reached final skill-score values of 0.77 and 0.71 for LCA00564 and LCA00566, respectively, indicating good agreement with the observed trajectories. For LCA00565, however, the final skill score was 0.04, reflecting the model's limited ability to reproduce nearshore trajectories over the shallow continental shelf. These results highlight that the IBI model captures the broader shelf-edge circulation more successfully than the fine-scale nearshore dynamics.

The horizontal scale and the mean location of the cyclonic circulation cell were estimated independently from drifter trajectories and the relative vorticity field. These three approaches provided a consistent horizontal scale of approximately 40-45 km (Fig. S1), supporting the spatial coherence of the observed structure.

This confirms a well-defined cyclonic structure in the eastern sector of the Gulf of Cádiz, active throughout most of the analysed period. These calculations were used to select a central reference point (36.81° N, 7.57° W) in order to analyse the temporal evolution of the vertical current velocity within the core of the cyclonic cell.

The temporal evolution of the vertical velocity at this point was examined for October 2022 (Fig. 11). Positive values (blue colours) indicate upward motions associated with upwelling processes, whereas negative values (reddish tones) represent downward movements.

During the period when the cyclonic circulation cell was recorded by the drifters (approximately between 12 and 23 October), persistent positive vertical velocities were observed, extending to depths greater than 300 m, suggesting a significant upward movement of subsurface water masses towards the surface. These upwelling events coincide temporally with the development of the cyclonic circulation cell described previously, demonstrating the ability of this structure to generate vertical motions within its core.

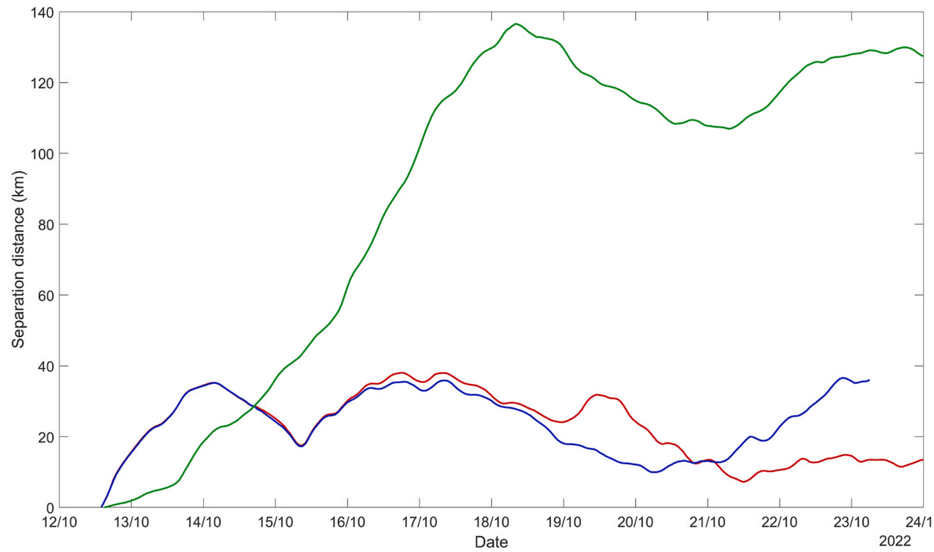

Fig. 10. Separation distance (km) between the observed and IBI-simulated trajectories for each drifter over time: green (LCA00565), red (LCA00564), and blue (LCA00566). (For interpretation of the references to colour in this figure legend, the reader is referred to the Web version of this article.)

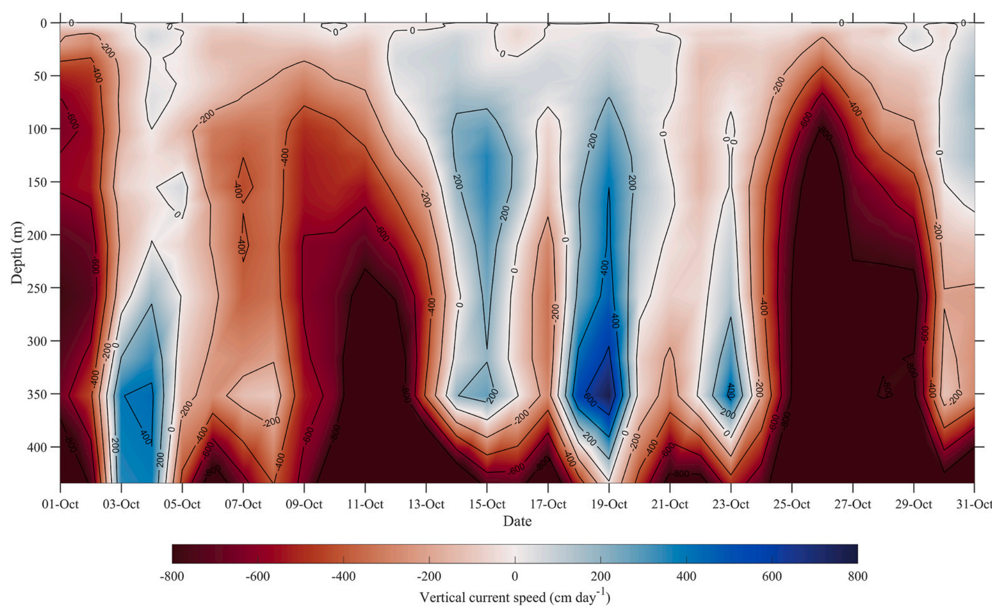

Fig. 11. Temporal evolution of vertical velocity (cm day^{-1}) at the central point of the cyclonic circulation cell (36.81°N, 7.57°W) during October 2022, from 450 m depth to the surface. Positive values (blue tones) indicate upward motions associated with upwelling processes, while negative values (reddish tones) represent downward movements. (For interpretation of the references to colour in this figure legend, the reader is referred to the Web version of this article.)

3.5. Particle dispersion modelling

Fig. 12 shows the complete trajectories of particles released from two initial positions: Position 1 (37.07° N, 7.42° W), shown in orange, and Position 2 (36.95° N, 7.42° W), shown in blue. The three regions defined for the dispersion analysis are also indicated: Western Shelf, Cyclonic Cell and Off Shelf. These regions were delineated to examine patterns of particle transport, retention, and export in the coastal zone.

A total of 32 particles were released for each position. For Position 1, 7 particles (21.9%) ended within the Cyclonic Cell, 21 particles (65.6%) remained on the Western Shelf, east of CSM, and 4 particles (12.5%) were advected towards the Off Shelf region. For Position 2, 13 particles (40.6%) reached the Cyclonic Cell, 1 particle (3.1%) remained on the Western Shelf, and 18 particles (56.3%) were transported offshore into the Off Shelf region.These results indicate clear differences in dispersion patterns between the two release positions. Particles released from Position 1 showed greater retention over the continental shelf, whereas those released from Position 2 showed enhanced export towards oceanic waters. This suggests that the cyclonic circulation cell influences surface-water connectivity and redistribution in the study area.

Retention time within the Cyclonic Cell was also analysed. To ensure that trajectories were long enough for comparison, only the first ten particles from each release position were considered, each considering at least 11 days of simulation. None of the particles released from Position 1 remained trapped within the Cyclonic Cell during the analysed period. Conversely, particles released from Position 2 showed retention times ranging from 8.8 to 16 days, with an average of 12.59 days. The retention times indicate that some particles were eventually exported from the Cyclonic Cell by the prevailing circulation.

A supplementary video showing the complete evolution of the

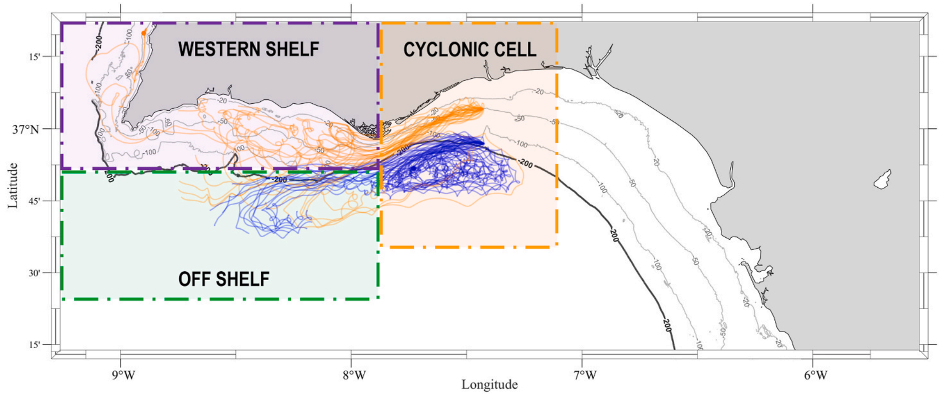

Fig. 12. Complete trajectories of particles released from two initial positions: Position 1 (37.07° N, 7.42° W), shown in orange, and Position 2 (36.95° N, 7.42° W), shown in blue. The three regions used for the dispersion analysis are shown: Western Shelf (purple) Cyclonic Cell (orange), and Off Shelf (green). (For interpretation of the references to colour in this figure legend, the reader is referred to the Web version of this article.)

particle trajectories throughout the simulation period is provided in the Supplementary Material.

4. Discussion

Surface circulation in the GoC is a highly dynamic and complex system driven by the interaction of multiple physical processes, including wind forcing, bathymetric constrains, and regional current systems. The results of this case study provide new empirical evidence that improves the current understanding of mesoscale and submesoscale circulation patterns, particularly east of CSM. The cyclonic circulation cell is identified in this study, with a horizontal scale of approximately 40–45 km and a duration of about 12 days during the analysed period, is consistent with a mesoscale feature. In contrast, the fine-scale SST and Chl-*a* gradients observed along the edges of the cell, including filaments and frontal structures, are suggestive of submesoscale variability at horizontal scales of ∼1–10 km. However, a full characterization of these submesoscale processes lies beyond the resolution of the available satellite products and the IBI model. This interpretation was achieved through an integrated approach combining drifter trajectories, satellite observations, atmospheric simulations, and ocean model outputs.

The drifter trajectories recorded in October 2022 revealed a coherent cyclonic circulation cell east of the CSM, with an approximate diameter of 40-45 km (Fig. S1). Similar features have previously been described in numerical simulations (Peliz et al., 2014; Laiz et al., 2020) and inferred from thermal and oceanographic observations (García-Lafuente et al., 2006; Criado-Aldeanueva et al., 2006). The present study provides the direct *in situ* observational support for this circulation pattern.

The surface flow over the continental shelf of the GoC generally moves southeastward. However, under specific wind and pressure gradient conditions, flow reversals can occurs (e.g., Garel et al., 2016), favouring the development of cyclonic circulation. Recent studies have demonstrated that the intensification and westward extension of the CCC are strongly influenced by the zonal component of the wind, as well as by remote atmospheric pressure fluctuations over the western Mediterranean, particularly in the Ligurian Sea (Fanelli et al., 2024; Sirviente et al., 2023).

Criado-Aldeanueva et al. (2006) described a cyclonic cell over the continental shelf of the GoC, formed by the westward flowing CCC along the eastern shelf and its eastward recirculation near the CSM. The formation and dynamics of this recirculation appear to be modulated by local bathymetry and atmospheric forcing. Off CSM, the continental shelf is extremely narrow, less than 5 km wide, and the slope descends abruptly to depths exceeding 600 m (García-Lafuente and Ruiz, 2007). This topographic transition can channel the flow and concentrate kinetic energy, favouring localised current intensification. The acceleration observed in the drifter trajectories around the 80 m isobath coincides with this steep bathymetric gradient, suggesting that topography acts as a dynamical boundary that steers and locally strengthens the recirculation.

The temporal evolution of relative vorticity along the drifter tracks (Fig. S2) further supports the role of bathymetry as a dynamical factor influencing the cyclonic circulation cell. Drifters LCA00564 and LCA00566 crossed the steep continental shelf edge off CSM around 16th October, coinciding with a rapid increase in depth from approximately 150-200 m to more than 600 m. During this transition, the drifter derived relative vorticity increased. This behaviour is consistent with potential-vorticity adjustment over steep topography: as the water column is stretched across the shelf-slope transition, changes in relative vorticity may occur in response to the strong bathymetric gradient. This suggests that the topographic transition at the edge of the CSM continental shelf not only steers and accelerates the current, as indicated by the drifter velocities, but may also contribute to the local intensification of cyclonic vorticity and to the confinement of the circulation cell.

During the study period, alternating easterly and westerly winds were recorded (Fig. 4), reflecting the high atmospheric variability of the GoC in autumn. These winds generated alternating favourable and unfavourable conditions for coastal upwelling. The SST maps reveal a well-developed CCC, up to 3 °C warmer than the surrounding waters, coinciding with the ascending branch of the cyclonic circulation cell. This pattern is consistent with previous descriptions by Relvas and Barton (2002) and supports the coupling between wind forcing and mesoscale surface circulation.

The analysis of preceding wind conditions (Table 3) shows that easterly winds predominated in the southern sector of the GoC during early October, favouring the development of the CCC (Relvas and Barton, 2002; Vargas et al., 2003). Several authors have highlighted the important role of easterly winds in CCC formation (Relvas and Barton, 2002; Sánchez et al., 2006), and Teles-Machado et al. (2007) showed that the CCC intensifies under easterly forcing and weakens or disappears during westerly episodes. Other studies, however, suggest that the CCC can also originate or be reinforced by coastal pressure gradients generated during the relaxation of upwelling-favourable winds (Garel et al., 2016; Sirviente et al., 2023). In this context, the alternation between easterly and westerly episodes may induce a transition between a westward-directed CCC and an eastward recirculation, contributing to the closure of the cyclonic cell east of the CSM (García-Lafuente et al., 2006).

If easterlies winds persist for a prolonged period, the CCC can skirt the CSM and extend towards the western sector of the GoC (Fiúza, 1983). In the present study, the shift to westerlies winds recorded in mid-October (Fig. 4) appears to have favoured eastward recirculation and the development of the described cyclonic circulation cell described here. This change in wind direction modified the surface Ekman

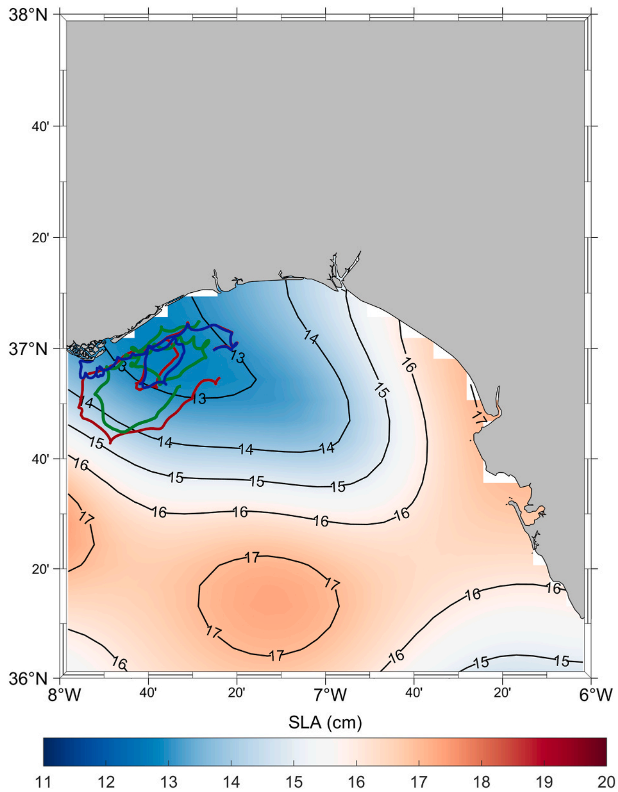

Fig. 13. Mean Sea Level Anomaly (SLA) over the Gulf of Cádiz during 12–24 October 2022. Coloured lines represent the trajectories of the three drifters from their release on 12th October 2022 to the end of the period: green (LCA00565), red (LCA00564), and blue (LCA00566). (For interpretation of the references to colour in this figure legend, the reader is referred to the Web version of this article.)

transport, generating divergence and upward motion along the eastern margin and coinciding with the intensification of the cyclonic circulation.

The mean SLA field for the study period (Fig. 13) shows an area of relatively low sea level in the northwestern sector of the GoC, surrounded by higher values towards the south and east. This pattern defines a horizontal sea-level gradient consistent with cyclonic circulation. The spatial correspondence between the lower SLA region and the drifter trajectories confirms that the cyclonic circulation cell was also detectable in the satellite altimetry data, supporting the presence of a mesoscale dynamical signal (cyclonic circulation cell) during mid-October 2022.

Southwesterly winds, reaching up to 13 $m\,s^{-1}$, were strong enough to induce offshore Ekman transport and favour the upwelling of colder subsurface waters. This mechanism is similar to that described by Cravo et al. (2013) for upwelling events along the southwestern Iberian margin. The Ekman pumping calculations (Fig. 7) showed positive vertical velocities of up to $4 \times 10^{-5}\,m\,s^{-1}$, approximately six times higher than the mean autumnal values reported by de Oliveira Júnior et al. (2024). This difference is consistent with the occurrence of an intense and localised upwelling event, in contrast with the mean seasonal conditions analysed by those authors.

These atmospheric and oceanographic conditions likely enhanced the upward transport of colder, nutrient-rich waters, which would explain the thermal gradients observed in the SST maps (Fig. 6) and the increased Chl-*a* concentration within the cyclonic circulation cell (Fig. 5). Although the main circulation feature is mesoscale, submesoscale filaments and frontal structures are likely embedded within it, as suggested by the fine-scale SST and Chl-*a* gradients.

The satellite imagery supports this interpretation, as the area east of CSM has previously been identified as a region with a high probability of upwelling based on the analysis of more than 3000 daily SST and Chl-*a* images (Ruiz and Navarro, 2006). This upwelling responds rapidly to changes in local wind conditions and tends to weaken or disappear when easterly conditions return (Criado-Aldeanueva et al., 2006).

In this study, the spatial coincidence between cooler waters and elevated Chl-a concentrations within the cyclonic circulation cell (Figs. 5 and 6) suggests a two-phase sequence. During the initial phase, from 14th to 18th October, the cyclonic circulation cell may have favoured the uplift and retention of subsurface waters offshore, concentrating biomass within its recirculation zone. During the subsequent phase, from 20th October onward), wind-induced coastal upwelling intensified, favouring the nearshore confinement of the cold, Chl-*a*-rich water mass that had previously retained within the cyclonic circulation cell.

The positive vertical velocities simulated by the IBI model within the cyclonic circulation cell (Fig. 11) are consistent with the presence of upward motions capable of transporting nutrients from deeper layers towards the surface. This result supports a close interaction between mesoscale circulation, coastal upwelling, and surface productivity. Similar processes have been described in other regions. For example, in the Gulf of Guinea, Thiam et al. (2024) documented a quasi-stationary cyclonic circulation cell that modulated the intensity of coastal upwelling. Although the dynamical settings differ, both systems demonstrate how mesoscale cyclonic circulations can favour the upward transport of subsurface waters and the retention or recirculation of coastal waters, thereby modulating the intensity and spatial extent of upwelling.

The coincidence between the drifter trajectories and the offshore displacement of the Chl-*a*-rich filament suggests that the net transport associated with the circulation and upwelling may explain part of the observed motion, particularly that of drifter LCA00564. On 19 October, this drifter moved south-southeastwards against the predominant wind direction (Table 3), which would have favoured north-northeastward advection if direct wind forcing had dominated. This suggests that its trajectory was primarily controlled by mesoscale circulation rather than by direct wind forcing alone. This behaviour agrees with the observations of García et al. (2002), who related local upwelling events and circulation near CSM to the spatial distribution of biological variables.

The Lagrangian particle analysis (Fig. 12) highlights the role of mesoscale structures in the redistribution of water masses along the continental margin. Part of the released particles were advected off the shelf, while others remained temporarily trapped within the cyclonic circulation cell, with residence times of up to approximately two weeks. This behaviour suggests that such structures can act as mechanisms of lateral mixing and transport, exporting coastal waters towards more oceanic regions.

Because shelf waters are typically enriched in nutrients and organic matter, their advection towards more oligotrophic areas may fertilise the open sea and modify local biogeochemical properties (Fennel, 2010). Processes of this kind, driven by recirculation and partial water mass retention, are common along continental margins and contribute to the lateral transport of nutrients, organic matter, and trace metals (Laiz et al., 2020). In this context, the cyclonic circulation cell identified in this study may act as an interface between coastal and open-ocean domains. Furthermore, recent observations in the GoC indicate that such processes can also facilitate the transport and redistribution of microplastics and other contaminants along the continental margin (Laiz et al., 2024), reinforcing the relevance of mesoscale features for the physical and biogeochemical dynamics of the system.

The formation and modulation of the cyclonic circulation cell can be interpreted as the result of interactions between atmospheric forcing, bathymetry, and mesoscale dynamics. Easterly winds favour the development of the CCC, which flows westwards along the eastern shelf of the GoC (e.g., Relvas and Barton, 2002; Garel et al., 2016). Subsequent shifts to westerly or southwesterly winds may weaken or reverse this westward flow near CSM, favouring the development of a cyclonic recirculation in this region (García-Lafuente et al., 2006; Teles-Machado et al., 2007; de Oliveira Júnior et al., 2022). The abrupt topographic transition at the edge of the continental shelf off the CSM may act both as a geographical boundary that helps constrain the circulation (García-Lafuente and Ruiz, 2007) and as a dynamical factor influencing the vorticity field. The increase in relative vorticity observed along the drifter tracks when crossing the shelf-slope region is consistent with potential vorticity adjustment over steep topography (Pedlosky, 1987), suggesting that the bathymetric gradient may contribute to the local intensification of cyclonic vorticity and to the confinement of the circulation cell, rather than acting solely as a passive boundary.

Once established, the circulation cell is associated with positive Ekman velocities (Fig. 7), which are consistent with upward transport of nutrient-rich subsurface waters and with the observed coupling between physical and biogeochemical dynamics (Cravo et al., 2013; Oliveira et al., 2024). The vertical velocities simulated by the IBI model within the cell interior are also consistent with this upwelling signal. However, their absolute magnitude should be interpreted with caution, as they reflect not only wind-driven Ekman pumping but also flow–topography interactions and other dynamical contributions (Jacox et al., 2018; Mazzini and Barth, 2013). This conceptual framework links the atmospheric, topographic, and mesoscale controls of the observed event, while highlighting the need for further analyses to assess whether similar mechanisms operate recurrently in the region.

Finally, the evaluation of the high-resolution IBI model shows that it reproduces the main characteristics of the observed cyclonic circulation, including the areas of maximum acceleration off CSM and along the edges of the cyclonic circulation cell (Fig. 8), with velocities comparable to those recorded by the drifters (Fig. 3). The quantitative assessment using the Lagrangian skill score of Liu and Weisberg (2011) supports this model performance for drifters released near the shelf edge. However, the model performed poorly for the drifter released over the shallower continental shelf, indicating limitations in its ability to reproduce fine-scale nearshore dynamics.

Although small spatial discrepancies were detected, such as a slight southward displacement of the simulated cyclonic circulation cell relative to the drifter trajectories, the overall coherence between both datasets suggests that the IBI model is useful for analysing the evolution and dynamics of similar mesoscale structures. Nevertheless, the model's horizontal resolution of approximately 3 km may limit its ability to fully capture the smaller-scale features present within the cyclonic circulation cell. In addition, the vertical velocities obtained from the IBI model are larger than those estimated from Ekman pumping. This is consistent with the fact that Ekman pumping provides only a first-order estimate of wind-driven vertical transport and does not capture all the processes contributing to vertical motion in coastal systems (Jacox et al., 2018). The model-derived vertical velocities reflect the combined action of different dynamical processes, including wind forcing and flow–topography interaction, which play an important role in the variability of coastal upwelling (Mazzini and Barth, 2013). Accordingly, these values should be interpreted with caution in terms of their absolute magnitude. Nevertheless, the model results describe the spatial patterns and relative variability of vertical motions associated with the cyclonic circulation cell. Moreover, the model provides valuable information in areas or periods where field data are scarce, complementing the spatial and temporal gaps inherent to *in situ* observations.

Given the limited availability of direct measurements in the GoC, combining targeted oceanographic field campaigns with high-resolution numerical output, such as those provided by the IBI model, represents an effective strategy to improve understanding of small-scale circulation and its coupling with marine productivity in the region.

5. Conclusions

This study provides direct *in situ* observational evidence of a cyclonic circulation cell east of CSM in the northern GoC. By combining Lagrangian drifters, satellite imagery, and high-resolution numerical simulations, a coherent cyclonic circulation cell approximately 40-45 km in diameter was identified during October 2022. Although the main circulation feature is mesoscale in scale, submesoscale filaments and frontal structures are likely embedded within it, as suggested by the fine-scale gradients observed in the SST and Chl-a fields.

The drifter trajectories revealed alternating eastward and westward flows modulated by wind variability, bathymetric steering, and mesoscale dynamics. The WRF simulations indicate that alternating easterly and westerly winds played an important role in circulation reversals, while the IBI model reproduced the main features of the cyclonic circulation cell and the associated flow accelerations near the shelf break. However, model performance was better for drifters released near the shelf edge than for the drifter released over the shallow continental shelf, highlighting the limitations of the model in resolving fine-scale nearshore dynamics.

The results provide new empirical evidence that the interaction between atmospheric forcing, local bathymetry, and upwelling processes governs small-scale circulation in the northern GoC. Westerly winds during mid-October 2022 induced local upwelling east of CSM, generating positive Ekman pumping and promoting the ascent of subsurface waters. The coexistence of cold waters and enhanced Chl-a concentrations within the cyclonic circulation cell core supports the interpretation of an active cyclonic recirculation that modulates both the physical structure and the surface productivity of the region. These findings provide new insights into the dynamics of the CCC and its coupling with mesoscale variability and cross-shelf exchanges along the Iberian margin.

Beyond its physical relevance, the observed cyclonic structure represents an active interface between coastal and open-ocean domains, with potential implications for biological productivity, pollutant dispersion, and cross-shelf connectivity. The strong agreement between observations and numerical simulations highlights the value of integrating *in situ* measurements, satellite data, and model analyses to characterize mesoscale circulation in coastal environments. Future work should aim to expand the observational database through new Lagrangian experiments and complementary oceanographic surveys, and to improve model resolution in order to capture transient submesoscale structures and assess their role in biogeochemical exchanges and coastal ecosystem dynamics.

CRediT authorship contribution statement

Esther Luján-Amoraga: Data curation, Formal analysis, Investigation, Writing – original draft. **Carlos Román-Cascón:** Conceptualization, Formal analysis, Funding acquisition, Project administration, Supervision, Writing – review & editing. **Juan Alberto Jiménez Rincón:** Conceptualization, Formal analysis, Writing – review & editing. **Alfredo Izquierdo:** Writing – review & editing. **Miguel Bruno:** Writing – review & editing. **Águeda Vázquez:** Funding acquisition, Writing – review & editing. **Paulo Relvas:** Writing – review & editing. **Erwan Garel:** Writing – review & editing. **Marina Bolado-Penagos:** Conceptualization, Formal analysis, Supervision, Writing – review & editing.

Declaration of competing interest

The authors declare that they have no known competing financial interests or personal relationships that could have appeared to influence the work reported in this paper.

Acknowledgements

This work, has been carried out within the framework of the grant CNS2023-144885, funded by MICIU/AEI/10.13039/501100011033 and the European Union NextGenerationEU/PRTR through the

WIND4US project.

This study also forms part of the BRISA project (PID2024-159841OA-I00), and the project PID2023-150230NB-C21, *"Coastal biogeochemical exchange through the Strait of Gibraltar under climate change conditions."*, funded by the Spanish Government. Esther Luján-Amoraga was supported by a grant from the University of Ferrara and the University of Cadiz.

Marina Bolado-Penagos acknowledges support from the DGP POST 2024 00907 grant, funded by the Junta de Andalucía/CUII and co-financed by the European Social Fund Plus (FSE+).

Appendix A. Supplementary data

Supplementary data to this article can be found online at https://doi.org/10.1016/j.marenvres.2026.108321.

Data availability

Data will be made available on request.

References

Aguiar, E., Mourre, B., Juza, M., Reyes, E., Hernández-Lasheras, J., Cutolo, E., Mason, E., Casas, B., Escudier, R., Gómara, S., Beltrán, J.P., Sebastián, K., Lora, S., Frontera, B., Garau, B., Troupin, C., Torner, M., Heslop, E., Tintoré, J., 2020. Multi-platform model assessment in the Western Mediterranean Sea: impact of downscaling on the surface circulation and mesoscale activity. Ocean Dyn. 70, 273–288. https://doi.org/10.1007/s10236-019-01317-8.

Bolado-Penagos, M., González, C.J., Chioua, J., Sala, I., Gómiz-Pascual, J.J., Vázquez, Á., Bruno, M., 2020. Submesoscale processes in the coastal margins of the Strait of Gibraltar. The Trafalgar–Alboran connection. Prog. Oceanogr. 181, 102219. https://doi.org/10.1016/j.pocean.2019.102219.

Brink, K.H., 2016. Cross-shelf exchange. Ann. Rev. Mar. Sci 8, 59–78. https://doi.org/10.1146/annurev-marine-010814-015717.

Cravo, A., Relvas, P., Cardeira, S., Rita, F., 2013. Nutrient and chlorophyll a transports during an upwelling event in the NW margin of the Gulf of Cadiz. J. Mar. Syst. 128, 208–221. https://doi.org/10.1016/j.jmarsys.2013.05.001.

Criado-Aldeanueva, F., García-Lafuente, J., Vargas, J.M., Del Río, J., Vázquez, A., Reul, A., Sánchez, A., 2006. Distribution and circulation of water masses in the Gulf of Cádiz from *in situ* observations. Deep Sea Res. Part II Top. Stud. Oceanogr. 53 (11–13), 1144–1160. https://doi.org/10.1016/j.dsr2.2006.04.009.

de Oliveira Júnior, L., Garel, E., Relvas, P., 2021. The structure of incipient coastal counter currents in South Portugal as indicator of their forcing agents. J. Mar. Syst. 214, 103486. https://doi.org/10.1016/j.jmarsys.2020.103486.

de Oliveira Júnior, L., Relvas, P., Garel, E., 2022. Kinematics of surface currents at the northern margin of the Gulf of Cádiz. Ocean Sci. 18 (4), 1183–1202. https://doi.org/10.5194/os-18-1183-2022.

de Oliveira Júnior, L., Relvas, P., Garel, E., 2024. Upwelling processes variability and water circulation along the northern margin of the Gulf of Cádiz. Cont. Shelf Res., 105310 https://doi.org/10.1016/j.csr.2024.105310.

Delandmeter, P., van Sebille, E., 2019. The parcels v2.0 Lagrangian framework: new field interpolation schemes. Geosci. Model Dev. 12, 3571–3584. https://doi.org/10.5194/gmd-12-3571-2019.

Dong, C., You, Z., Dong, J., Ji, J., Sun, W., Xu, G., Lin, X., Yang, Y., Zhou, C., Zhang, Z., 2025. Oceanic mesoscale eddies. Ocean Land Atmos. Res. 4, 81. https://doi.org/10.34133/olar.0081.

Dudhia, J., 1989. Numerical study of convection observed during the Winter Monsoon experiment using a mesoscale two-dimensional model. J. Atmos. Sci. 46, 3077–3107. https://doi.org/10.1175/1520-0469(1989)046.

Fanelli, C., Gomiz Pascual, J.J., Bruno-Mejías, M., Navarro, G., 2024. Using a combination of high-frequency coastal radar dataset and satellite imagery to study the patterns involved in the coastal countercurrent events in the Gulf of Cádiz. Remote Sens. 16 (4), 687. https://doi.org/10.3390/rs16040687.

Fennel, K., 2010. The role of continental shelves in nitrogen and carbon cycling: northwestern North Atlantic case study. Ocean Sci. 6, 539–548. https://doi.org/10.5194/os-6-539-2010.

Fiúza, A.F.G., 1983. Upwelling patterns off Portugal. In: Coastal Upwelling: Its Sediment Record. Part A: Responses of the Sedimentary Regime to Present Coastal Upwelling. Springer, US, Boston, MA, pp. 85–98. https://doi.org/10.1007/978-1-4615-6651-9_5.

Fu, L.L., Chelton, D.B., Le Traon, P.-Y., Morrow, R., 2010. Eddy dynamics from satellite altimetry. Oceanography (Wash. D. C.) 23 (4), 14–25. https://doi.org/10.5670/oceanog.2010.02.

García, C.M., Prieto, L., Vargas, M., Echevarría, F., García-Lafuente, J., Ruiz, J., Rubin, J.P., 2002. Hydrodynamics and the spatial distribution of plankton and TEP in the Gulf of Cádiz (SW Iberian Peninsula). J. Plankton Res. 24 (8), 817–833. https://doi.org/10.1093/plankt/24.8.817.

García-Lafuente, J., Delgado, J., Criado-Aldeanueva, F., Bruno, M., del Río, J., Vargas, J.M., 2006. Water mass circulation on the continental shelf of the Gulf of Cádiz. Deep Sea Res. Part II Top. Stud. Oceanogr. 53 (11–13), 1182–1197. https://doi.org/10.1016/j.dsr2.2006.04.011.

García-Lafuente, J., Ruiz, J., 2007. The Gulf of Cádiz pelagic ecosystem: a review. Prog. Oceanogr. 74 (2–3), 228–251. https://doi.org/10.1016/j.pocean.2007.04.001.

Garel, E., Laiz, I., Drago, T., Relvas, P., 2016. Characterization of coastal counter-currents on the inner shelf of the Gulf of Cádiz. J. Mar. Syst. 155, 19–34. https://doi.org/10.1016/j.jmarsys.2015.11.001.

GCOS (Global Climate Observing System), 2016. The Global Observing System for Climate: Implementation Needs, 200. World Meteorological Organization (WMO), p. 316. GCOS Report No.

Gomis, D., Ruiz, S., Pedder, M.A., 2001. Diagnostic analysis of the 3D ageostrophic circulation from a multivariate spatial interpolation of CTD and ADCP data. Deep Sea Res. Oceanogr. Res. Pap. 48 (1), 269–295. https://doi.org/10.1016/S0967-0637(00)00052-1.

Greene, C.A., Thirumalai, K., Kearney, K.A., De Wever, A., 2019. The climate data toolbox for MATLAB. Geosci. Model Dev. 12, 3785–3807. https://doi.org/10.5194/gmd-12-3785-2019.

Hong, S.-Y., Dudhia, J., Chen, S.-H., 2004. A revised approach to ice microphysical processes for the bulk parameterization of clouds and precipitation. Mon. Weather Rev. 132, 103–120. https://doi.org/10.1175/1520-0493(2004)132.

Hong, S.-Y., Noh, Y., Dudhia, J., 2006. A new vertical diffusion package with explicit treatment of entrainment processes. Mon. Weather Rev. 134, 2318–2341. https://doi.org/10.1175/MWR3199.1.

Jacox, M.G., Edwards, C.A., Hazen, E.L., Bograd, S.J., 2018. Coastal upwelling revisited: Ekman, Bakun, and improved upwelling indices for the U.S. West Coast. J. Geophys. Res. Oceans 123, 7332–7350. https://doi.org/10.1029/2018JC014187.

Laiz, I., Foletti, N., Teles-Machado, A., Plecha, S., Peliz, A., Sánchez Leal, R.F., Bolado-Penagos, M., 2024. Spatial distribution of microplastics in the Gulf of Cádiz as a function of their density: a Lagrangian modelling approach. Sci. Total Environ. 950, 175212. https://doi.org/10.1016/j.scitotenv.2024.175212.

Laiz, I., Plecha, S., Teles-Machado, A., González-Ortegón, E., Sánchez-Quiles, D., Cobelo-García, A., Roque, D., Peliz, A., Sánchez-Leal, R.F., Tovar-Sánchez, A., 2020. The role of the Gulf of Cádiz circulation in the redistribution of trace metals between the Atlantic Ocean and the Mediterranean Sea. Sci. Total Environ. 719, 134964. https://doi.org/10.1016/j.scitotenv.2019.134964.

Large, W.G., Pond, S., 1981. Open ocean momentum flux measurements in moderate to strong winds. J. Phys. Oceanogr. 11 (3), 324–336. https://doi.org/10.1175/1520-0485(1981)011.

Liu, Y., Weisberg, R.H., 2011. Evaluation of trajectory modeling in different dynamic regions using normalized cumulative Lagrangian separation. J. Geophy. Res.: Oceans 116, C09013. https://doi.org/10.1029/2010JC006837.

Mazzini, P.L.F., Barth, J.A., 2013. A comparison of mechanisms generating vertical transport in the Brazilian shelf. J. Geophys. Res. Oceans 118, 5977–5993. https://doi.org/10.1002/2013JC008982.

McWilliams, J.C., 2016. Submesoscale currents in the ocean. Proceedings of the royal society A: mathematical. Phys. Eng. Sci. 472, 2189. https://doi.org/10.1098/rspa.2016.0117.

Mitchell, K.E., et al., 2005. The multi-institution North American Land Data Assimilation System (NLDAS): developing land surface models and building the data bases. Bull. Am. Meteorol. Soc. 86, 253–277. https://doi.org/10.1175/BAMS-86-3-253.

Mlawer, E.J., Taubman, S.J., Brown, P.D., Iacono, M.J., Clough, S.A., 1997. Radiative transfer for inhomogeneous atmospheres: RRTM, a validated correlated-k model for the longwave. J. Geophys. Res. Atmos. 102 (D14), 16663–16682. https://doi.org/10.1029/97JD00237.

Mulero-Martínez, R., Gómez-Enri, J., Mañanes, R., Bruno, M., 2021. Assessment of near-shore currents from CryoSat-2 satellite in the Gulf of Cádiz using HF radar-derived current observations. Rem. Sens. Environ. 256, 112310. https://doi.org/10.1016/j.rse.2021.112310.

NCAR (National Center for Atmospheric Research), 2023. The Weather Research & Forecasting Model (WRF): User Documentation. UCAR/NCAR, Boulder, Colorado. https://doi.org/10.5065/D6MK6B4K.

Pedlosky, J., 1987. Geophysical Fluid Dynamics, second ed. Springer-Verlag, New York, p. 710.

Peliz, A., Boutov, D., Barbosa Aguiar, A., Carton, X., 2014. The Gulf of Cadiz gap wind anticyclones. Cont. Shelf Res. 91, 171–191. https://doi.org/10.1016/j.csr.2014.09.004.

Peliz, A., Marchesiello, P., Santos, A.M.P., Dubert, J., Teles-Machado, A., Marta-Almeida, M., Le Cann, B., 2009. Surface circulation in the Gulf of Cádiz: 2. Inflow–outflow coupling and the Gulf of Cádiz slope current. J. Geophys. Res. Oceans 114 (3), C03011. https://doi.org/10.1029/2008JC004771.

Rautenbach, S.A., Mendes de Sousa, C., Carapuço, M., Relvas, P., 2024. High-resolution observations of the ocean upper layer south of Cape st. Vincent, the western northern margin of the Gulf of Cádiz. Earth Syst. Sci. Data 16, 4641–4654. https://doi.org/10.5194/essd-16-4641-2024.

Reggiannini, M., Janeiro, J., Martins, F., Papini, O., Pieri, G., 2021. Mesoscale patterns identification through SST image processing. In: Proceedings of the 2nd International Conference on Robotics, Computer Vision and Intelligent Systems (ROBOVIS 2021), pp. 165–172. https://doi.org/10.5220/0010714600003061.

Relvas, P., Barton, E.D., Dubert, J., Oliveira, P.B., Peliz, A., da Silva, J.C.B., Santos, A.M.P., 2007. Physical oceanography of the western iberia ecosystem: latest views and challenges. Prog. Oceanogr. 74 (2–3), 149–173. https://doi.org/10.1016/j.pocean.2007.04.021.

Relvas, P., Barton, E.D., 2002. Mesoscale patterns in the Cape São Vicente (Iberian Peninsula) upwelling region. J. Geophys. Res. Oceans 107 (C10), 3164. https://doi.org/10.1029/2000JC000456.

Relvas, P., Barton, E.D., 2005. A separated jet and coastal counter-flow during upwelling relaxation off Cape São Vicente (Iberian Peninsula). Cont. Shelf Res. 25 (1), 29–49. https://doi.org/10.1016/j.csr.2004.09.006.

Ribotti, A., Bussani, A., Menna, M., Satta, A., Sorgente, R., Cucco, A., Gerin, R., 2023. A Mediterranean drifter dataset. Earth Syst. Sci. Data 15, 4651–4659. https://doi.org/10.5194/essd-15-4651-2023.

Ruiz, J., Navarro, G., 2006. Upwelling spots and vertical velocities in the Gulf of Cádiz: an approach for their diagnose by combining temperature and ocean colour remote sensing. Deep Sea Res. Part II Top. Stud. Oceanogr. 53 (11–13), 1282–1293. https://doi.org/10.1016/j.dsr2.2006.04.012.

Sala, I., Navarro, G., Bolado-Penagos, M., Echevarría, F., García, C.M., 2018. High-chlorophyll-area assessment based on remote sensing observations: the case study of cape trafalgar. Remote Sens. 10 (2), 165. https://doi.org/10.3390/rs10020165.

Sirviente, S., Bolado-Penagos, M., Gomiz-Pascual, J.J., Romero-Cózar, J., Vázquez, A., Bruno, M., 2023. Dynamics of atmospheric-driven surface currents on the Gulf of Cádiz continental shelf and its link with the Strait of Gibraltar and the Western Alboran Sea. Prog. Oceanogr. 219, 103175. https://doi.org/10.1016/j.pocean.2023.103175.

Skamarock, W.C., Klemp, J.B., Dudhia, J., Gill, D.O., Liu, Z., Berner, J., Wang, W., Powers, J.G., Duda, M.G., Barker, D.M., Huang, X.Y., 2019. A description of the advanced research WRF model version 4. NCAR Tech. Note. https://doi.org/10.5065/1dfh-6p97.

Sánchez, R.F., Mason, E., Relvas, P., Da Silva, A.J., Peliz, A., 2006. On the inner-shelf circulation in the northern Gulf of Cádiz, southern Portuguese shelf. Deep Sea Res. Part II Top. Stud. Oceanogr. 53 (11–13), 1198–1218. https://doi.org/10.1016/j.dsr2.2006.04.010.

Sánchez, R.F., Relvas, P., 2003. Spring–summer climatological circulation in the upper layer of the cape st. Vincent region, southwest Portugal. ICES (Int. Counc. Explor. Sea) J. Mar. Sci. 60 (6), 1232–1250. https://doi.org/10.1016/S1054-3139(03)00138-3.

Sánchez-Leal, R.F., Bellanco, M.J., Naranjo, C., García-Lafuente, J., González-Pola, C., 2020. On the seasonality of waters below the seasonal thermocline in the Gulf of Cádiz. Cont. Shelf Res. 204, 104190. https://doi.org/10.1016/j.csr.2020.104190.

Soares, P.M.M., Cardoso, R.M., Semedo, Â., Chinita, M.J., Ranjha, R., 2014. Climatology of the Iberia coastal low-level wind jet: weather research forecasting model high-resolution results. Tellus Dyn. Meteorol. Oceanogr. 66 (1), 22377. https://doi.org/10.3402/tellusa.v66.22377.

Sydeman, W.J., García-Reyes, M., Schoeman, D.S., Rykaczewski, R.R., Thompson, S.A., Black, B.A., Bograd, S.J., 2014. Climate change and wind intensification in coastal upwelling ecosystems. Science 345 (6192), 77–80. https://doi.org/10.1126/science.1251635.

Talley, L.D., Pickard, G.L., Emery, W.J., Swift, J.H., 2011. Descriptive Physical Oceanography, sixth ed. Elsevier, Boston, p. 560.

Teles-Machado, A., Peliz, A., Dubert, J., Sánchez, R.F., 2007. On the onset of the Gulf of Cádiz Coastal countercurrent. Geophys. Res. Lett. 34 (12), L12610. https://doi.org/10.1029/2007GL030110.

Teles-Machado, A., Peliz, Á., McWilliams, J.C., Couvelard, X., Ambar, I., 2016. Circulation on the Northwestern Iberian margin: vertical structure and seasonality of the alongshore flows. Prog. Oceanogr. 140, 134–153. https://doi.org/10.1016/j.pocean.2015.05.021.

Thiam, A.K., Alory, G., Dadou, I., Napolitano, D., Aguedjou, H.M.A., Cardot, C., Morvan, G., Morel, Y., Jouanno, J., 2024. Mesoscale dynamics and its interaction with coastal upwelling in the northern Gulf of Guinea. Front. Mar. Sci. 11, 1500753. https://doi.org/10.3389/fmars.2024.1500753.

Trenberth, K.E., Large, W.G., Olson, J.G., 1990. The global ocean wind stress dataset: trends and variability. J. Phys. Oceanogr. 20 (3), 447–462. https://doi.org/10.1175/1520-0485(1990)020.

UCAR/NCAR, 2015. NCEP FNL (Final) operational global analysis data, 0.25° × 0.25. Res. Data Arch. Nat. Center Atmos. Res. https://doi.org/10.5065/D6M043C6.

Vargas, J.M., García-Lafuente, J., Delgado, J., Criado, F., 2003. Seasonal and wind-induced variability of sea surface temperature patterns in the Gulf of Cádiz. J. Mar. Syst. 38 (3–4), 205–219. https://doi.org/10.1016/S0924-7963(02)00280-4.